Rotating magnetic field actuation of a multicilia configuration

Dragos ISVORANU [1,*], Daniel IOAN [2], Petrisor Parvu [3]

* Corresponding author: Tel.: ++40 (0) 21 3250704; Email: ddisvoranu@gmail.com
1: Dept. of Thermodynamics, University Politehnica of Bucharest, RO, ddisvoranu@gmail.com
2: Lab. of Numerical Methods, University Politehnica of Bucharest, RO,daniel@lmn.pub.ro
3: Fac. of Aerospace Engineering, University Politehnica of Bucharest, RO, parvu@aero.pub.ro

Abstract The current paper continues the analysis of a completely novel method of fluid manipulation technology in micro-fluidics systems, inspired by nature, namely by the mechanisms found in ciliates. More information on this subject can be found at http://www.hitech-projects.com/euprojects/artic/. In order to simulate the drag forces acting on an array of artificial cilia, we have developed a computer code that is based on fundamental solutions of Stokes flow in a semi-infinite domain. The actuation mechanism consists of a bi-directional rotating excitation magnetic field. The magnetization induced by the magnetic field was calculated in a separate routine based on the Integral Nonlinear Equations Approach with 1D discretization of wire (cilium). Time averaged x-coordinate mass flow rates are computed for several cilium configurations resulting. The outcome and originality of this paper consist on assessing magnetic actuation as a practical tool for obtaining a consistent one-directional fluid flow.

Keywords: Artificial cilia, Micro Flow, Magnetic Actuation, Integral Nonlinear Equations

1. Introduction

The on-going miniaturization in a variety of scientific domains, especially in bio-chemistry and medicine, requires manipulation of progressively smaller volumes of biological fluids such as blood, saliva, urine, or polymer solutions. Examples of such applications are micro-channel cooling for electronics, inkjet printing for displays together with biomedical applications, controlled drug delivery systems and biosensors. Also, the nature of the manipulation may be quite broad: transportation, mixing, sorting, deforming, or rupturing. An attractive solution in partial fulfillment of these goals is represented by artificial cilia arrays. Cilia are thin hair-like cell appendices responsible for many essential biological functions. One of the most interesting and useful of these cilia functions is propulsion, meaning either self-propulsion of the organism or induction of fluid flow around a stationary organism at micron-scale dimensions. Theoretical research in this domain has mainly been devoted to understanding the biochemical engine driving such complex movements and providing valuable insights of the interaction between the deformations of the elastic structure and the viscous incompressible fluid surrounding it (Gueron and Liron, 1992; Gueron et.al, 1997; Gueron et.al., 1998; Gueron and Liron., 1999). Based on their typical dimensions and physical properties of biological fluids we are able to assess that the Reynolds number of such flows is of the order of unity or less. In this case not only is the flow laminar but it is dominated by viscous forces that make it close to a classical Stokes flow. On the other hand, the dynamics of such an elastic structure lacks the inertial term because of the very small characteristic mass. The movement of the individual cilia is asymmetric, i.e. a deformation cycle consists of an effective stroke and a recovery stroke. During the effective stroke the cilium behaves like a rigid rod while in the recovery stroke it bends and rolls back to the original position so that a resultant fluid transport in one direction is induced. Also, cilia operate collectively by hydrodynamic interaction that induces metachronal coordination, a slight phase lag of their movements generating a wave-like

aspect. Such behavior seems to aim at reducing energy expenditure per cycle beat.

Inducing sustainable one-direction flow with artificial cilia has several distinctive features comparing to the biological counterpart. The main issue is the different way of attaching the cilium to the support substrate. Contrary to the upright position of the natural cilium, the artificial one was tilted towards horizontal plane. The tilt angle may vary between 0 and 10-20 degrees. A flow efficiency analysis has showed better performance for an asymmetric geometric shape of the cilium associated with a harmonic actuation mechanism (Isvoranu et. al., 2008).

In the present paper we are investigating the main fluid flow features of an array of artificial cilia in a semi-infinite domain. As in the previous case (Isvoranu et.al., 2008), the actuation mechanism consists of a bi-directional rotating excitation magnetic field that interacts with the magnetized cilium. Velocity fields and lateral boundaries mass flow rates are computed for several cilia array configurations.

2. Physical model.

The cilium is modeled as an inextensible cylindrical filament of length L and circular cross section of radius a. The slenderness of the cilium is defined by ratio $\varepsilon = a/L \ll 1$. The center line of the filament is parameterized by its arc-length s ($0 \le s \le L$). The null value corresponds to the anchor point where the cilium is attached to the substrate surface; $s = L$ at the distal end. Two coordinate systems (CS) are defined, one fixed at the anchor and a Lagrangeean one attached to an arbitrary point on the cilium. Due to the axial symmetry in the magnetic field density we shall restrict our analysis to planar case. Hence, the coordinate systems are (x,y), global, and (T,N), local. The angle between the tangential direction in local CS and the x axis in global CS for each cilium in the array of K cilia is denoted $\alpha^{(k)}$, $k = 1,\ldots,K$, being a function of arc-length, time and $\alpha^{(k)} = \alpha^{(k)}(s,t)$. The parameterized equations of the center line points are given by

$$x^{(k)}(s,t) = \int_0^s \cos\left(\xi^{(k)},t\right)d\xi^{(k)} + x_0^{(k)},$$
$$y^{(k)}(s,t) = \int_0^s \sin\left(\xi^{(k)},t\right)d\xi^{(k)} \qquad (1)$$

where $x_0^{(k)}$ stands for the abscissa origin of each cilium of the array. The driving engine is represented by the magnetic torque $\mathbf{C}^{(k)} = \mathbf{C}^{(k)}(s,t)$. The response from the elastic structure is denoted by the shear force $\mathbf{F}^{(k)} = \mathbf{F}^{(k)}(s,t)$ and $\boldsymbol{\varphi}^{(k)} = \boldsymbol{\varphi}^{(k)}(s,t)$ are the viscous forces per unit length (drag forces) exerted by the surrounding fluid. Here and in the following the bold typeface denotes vector quantities. The velocity of the current cross section s of the arbitrary cilium (k) in the array is denoted by $\mathbf{V}^{(k)} = \mathbf{V}^{(k)}(s,t)$. From the mechanical point of view, we consider that each cilium is in mechanical equilibrium at every moment of time.

2.1. Equations of motion.

Considering a finite volume of an arbitrary cilium along the arc-length ds the balance of forces and moments in the local Frenet coordinate system reads:

$$\varphi_N^{(k)} = F_{N,s}^{(k)} + F_T^{(k)}\alpha_s^{(k)} \qquad (2)$$
$$\varphi_T^{(k)} = F_{T,s}^{(k)} - F_N^{(k)}\alpha_s^{(k)} \qquad (3)$$
$$C_{m,s}^{(k)} + F_N^{(k)} = EI\alpha_{ss}^{(k)} \qquad (4)$$

where subscripts N, T means normal and tangential components and s, t denote arc-length and time derivation. $C_{m,s}$ is the derivative of the magnetic torque. The drag force components are specified through linear dependence on velocity components

$$\varphi_N^{(k)} = -C_N V_N^{(k)} + g_N^{(k)}$$
$$\varphi_T^{(k)} = -C_T V_T^{(k)} + g_T^{(k)} \qquad (5)$$
$$g_N^{(k)} = C_N G_N^{(k)} \quad g_T^{(k)} = C_T G_T^{(k)} \qquad (6)$$

where $G_N^{(k)}$ and $G_T^{(k)}$ are the local CS components of the velocity induced at current location by the flow field generated by superposition of Stokes equation fundamental solutions and their image systems (Gueron

et.al., 1997). The normal and tangential specific drag coefficients are denoted by C_N and C_T. Time differentiation of geometrical relations (1) leads to kinematic conditions:

$$V_{N,s}^{(k)} = \alpha_t^{(k)} - V_T^{(k)}\alpha_s^{(k)} \quad (7)$$

$$V_{T,s}^{(k)} = V_N^{(k)}\alpha_s^{(k)} \quad (8)$$

2.2. Flow equations.

Taking into account that viscous forces prevail in this type of flow, the movement of the fluid can be modeled by superposition of the fundamental solutions of Stokes equations

$$\nabla p = \mu\Delta\mathbf{U} + \mathbf{f}, \quad \nabla\cdot\mathbf{U} = 0 \quad (9)$$

$$\mathbf{f} = \boldsymbol{\varphi}\delta(\mathbf{R}'-\mathbf{R}_O) \quad (10)$$

where p is pressure per unit length, μ the dynamic viscosity of the fluid, $\mathbf{U}$ velocity vector per unit length, $\boldsymbol{\varphi}$ the drag force per unit length acting at the point defined by position vector $\mathbf{R}_O$ (Gueron and Liron, 1992). In the local cartesian coordinates the velocity $\mathbf{V}^{(\mathbf{k})}$ of the cross section s_0, $q < s_0 < L - q$, reads

$$\mathbf{V}^{(k)}(s_0,t) = -\frac{1}{C_T}\varphi_T^{(k)}(s_0,t)\mathbf{t} - \frac{1}{C_N}\varphi_N^{(k)}(s_0,t)\mathbf{n} + \mathbf{G}^{(k)}(s_0,t) \quad (11)$$

$$\mathbf{G}^{(k)}(s_0,t) = \int_{|s-s_0|>q}\mathbf{U}_s\left(\mathbf{R}^{(k)}(s_0,t),\mathbf{R}'^{(k)}(s,t),-\boldsymbol{\varphi}^{(k)}(s,t)\right)ds + \int_{0\le s\le L}\mathbf{V}_{si}\left(\mathbf{R}^{(k)}(s_0,t),\mathbf{R}'^{(k)}(s,t),-\boldsymbol{\varphi}^{(k)}(s,t)\right)ds + \int_{0\le s\le L}\mathbf{V}_{di}\left(\mathbf{R}^{(k)}(s_0,t),\mathbf{R}'^{(k)}(s,t),-a^2\boldsymbol{\varphi}^{(k)}(s,t)/4\mu\right)ds + \sum_{j=1}^{K}\int_{0\le s\le L}\mathbf{U}_s\left(\mathbf{R}^{(k)}(s_0,t),\mathbf{R}'^{(j)}(s,t),-\boldsymbol{\varphi}^{(j)}(s,t)\right)ds \quad (12)$$

The drag coefficients

$$C_T = \frac{8\pi\mu}{-2+4\ln(2q/a)} \quad (13)$$

$$C_N = \frac{8\pi\mu}{1+2\ln(2q/a)} \quad (14)$$

are obtain after integrating the tangential velocity induced by the Stokeslets over a cuasi-cylindrical domain $[s_0-q, s_0+q]$ with an error of $O(a/q^2)$ (Gueron et.al., 1997).

2.3. Magnetostatic equations.

The magnetic actuation is produced by a rotating magnetic field generated longitudinal and transversal coils. Harmonic excitation of coils is assumed. Taking into account the negligible lateral dimension of the cilium, we infer z-axis symmetry of the magnetic field. In the present analysis, super paramagnetic material without hysteretic behavior was considered for the cilia.

The magnetization induced by an external magnetic field $\mathbf{H}_0$ in an arbitrary point P defined by the position vector $\mathbf{R}'$ of a single cilium has the expression (Jackson, 1974)

$$\mathbf{M}(\mathbf{R}') + \frac{\chi}{4\pi}\int_{\Omega_m}\nabla\cdot\mathbf{M}(\mathbf{R})\nabla\left[\frac{1}{|\mathbf{R}'-\mathbf{R}|}\right]dV = \chi\mathbf{H}_0(\mathbf{R}') \quad (15)$$

where Ω_m is the wire-flap volume, $\mathbf{M}$ magnetization, χ magnetic susceptibility ($\chi = \mu_r - 1$) and $\mathbf{R}$ the current position vector. Our previous analysis (Isvoranu et.al., 2008) yielded small self induction field in the technologically accepted range of [3.5-9] relative magnetic permeability. Hence, we have discarded the mutual self induced fields resulting in the same distribution of the induced magnetization for each cilium of the array of cilia. In order to evaluate the integral in (15) it is convenient to discretize the wire into N smaller control volumes Ω_i of length $2\Delta s$ over which the magnetization divergence can be approximated by the finite difference. Hence, we can rewrite (15) as

$$\mathbf{M}^j + \frac{\chi}{2}\sum_{i=1}^{N}\left[\frac{M_T^{i+1}-M_T^i}{2(s^{i+1}-s^i)}\right]\cdot\left[I_1^{j,i+1/2}\mathbf{t}^{i+1/2} + (I_2^{j,i+1/2}-I_3)\mathbf{n}^{i+1/2}\right] = \chi\mathbf{H}_0^j \quad (16)$$

where I_1, I_2 and I_3 are coefficients of influence resulted through basic calculus.

Once the magnetization vector $\mathbf{M}^j$ is known we are able to determine the self field

strength generated by this magnetization by simply neglecting the external field in eq. (16).

We finally get

$$\mathbf{H}_{self}^{j} = -\frac{1}{2}\sum_{i=1}^{N}\left[\frac{M_T^{i+1}-M_T^{i}}{2\left(s^{i+1}-s^{i}\right)}\right]\cdot \cdot\left[I_1^{j,i+1/2}\mathbf{t}^{i+1/2}+\left(I_2^{j,i+1/2}-I_3\right)\mathbf{n}^{i+1/2}\right] \quad (17)$$

Based on the constitutive relation we obtain the self field density

$$\mathbf{B}_{self} = \mu_0\mu_r\mathbf{H}_{self} \quad (18)$$

where μ_0, μ_r represents the magnetic permeability of the vacuum and the relative permeability of the super paramagnetic material. Hence, the magnetic torque reads

$$d\mathbf{C}_m^{i+1/2} = \mathbf{M}^{i+1/2}\times\left(\mathbf{B}_0^{i+1/2}+\mathbf{B}_{self}^{i+1/2}\right)dV^{i} \quad (19)$$

Numerical derivation of the magnetic torque has been used in order to ensure the normal equilibrium condition (4).

2.4. Magnetic actuation

The rotating magnetic field $\mathbf{B}_0 = \left(B_{x,}B_y\right)$ is modeled by the following time dependence

$$B_x(t) = B\sin(2\pi ft)$$
$$B_y(t) = B\sin\left(2\pi ft+\frac{\pi}{12}\right) \quad (20)$$

where f is frequency.

3. Numerical approach

The derivative of magnetic torque used in the equilibrium condition (4) provides the active force denoted by

$$S = \frac{dC_m}{ds} \quad (21)$$

After proper non-dimensionalization a system of integro-differential equations has to be solved in order to account for the fluid-structure interaction (Gueron et.al., 1997; Isvoranu et.al., 2008). Based on an adequate linear discretization of the arc-length of each wire (31 segments, for example) and using a Crank-Nicholson finite difference scheme, the system is solved for the time-dependent parameterization of the array of artificial cilia $\alpha^{(k)} = \alpha^{(k)}(s,t)$. The same boundary conditions as in (Isvoranu et.al., 2008) are imposed. As for initial conditions, we have

$$\alpha^{(k)}(0,0) = \pi/18$$
$$\alpha^{(k)}(s,0) = \frac{\pi}{18}+\frac{\pi}{18(N-1)}\left(10.5-s\frac{N}{L}\right) \quad (22)$$

for $s > 0$.

A typical discretization of the fluid domain surrounding the cilium using a rectangular grid is depicted in Figure 1.

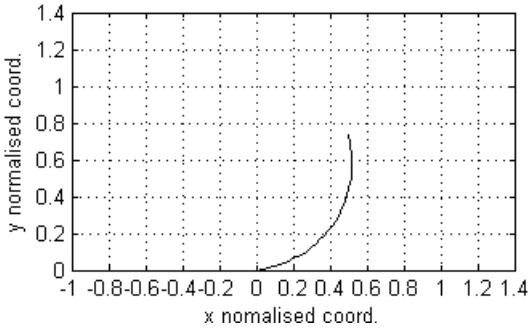

Figure 1. Geometry and grid.

The velocity field $\mathbf{V}(v_x, v_y)$ in this domain is calculated based on the singular solution of Stokes equation (Stokeslet) for all nodes of the grid (x_g, y_g).

$$\mathbf{V}(x_g, y_g, t) = \sum_{k=1}^{K}\int_{0\le s\le L}\mathbf{U}_s\left(\mathbf{R}(x_g, y_g), \mathbf{R}'^{(k)}(s,t), -\boldsymbol{\varphi}^{(k)}(s,t)\right)ds \quad (23)$$

Using this velocity field we are able to determine the x-coordinate mass flow rate generated by the magnetic actuation of the cilium in every section $x = ct$ of the domain.

$$\dot{m}_x = L\rho_w\int_{y=0}^{y=1.5}v_x dy \quad (24)$$

where ρ_w is the density of water.

4. Results.

A computer code has been devised in order to perform the necessary simulations. All external inputs and the range of other parameters variations have been imposed so as to ensure mechanical and geometrical stability. The external parameters are presented in Table 1. A first investigation was performed in order

to assess the flow field pattern. Snapshots of the streamlines distribution have been plotted

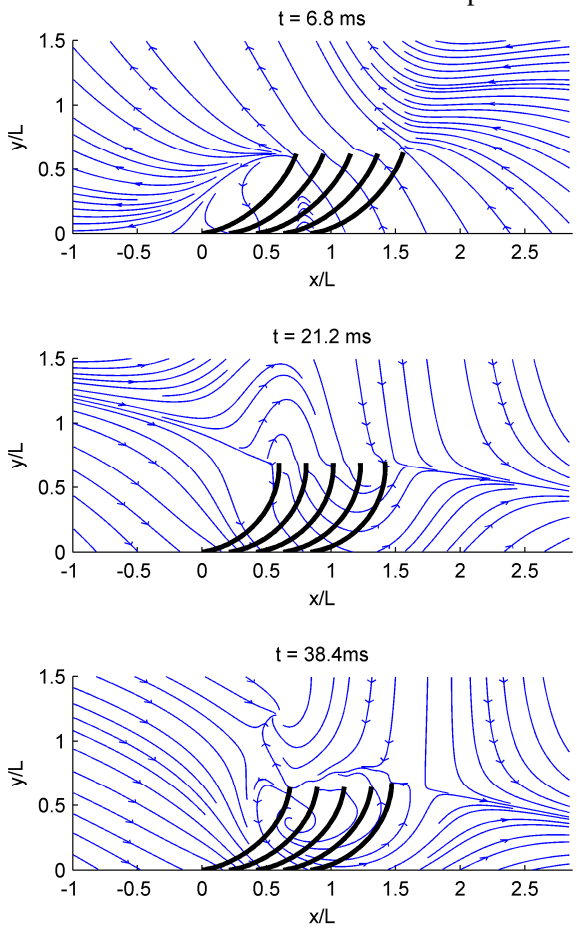

Figure 2. Five cilia array streamlines distribution. Spacing 0.21.

in Figure 2 at different moments of time for a 5 cilia array configuration.

Table 1

Parameter	L	a	q	f	μ
Value	100	1	10	25	0.001
Unit	μm	μm	μm	Hz	Ns/m^2
Parameter	E	$B_x=B_y$	ρ_w	μ_0	
Value	10^6	0.01	1000	$4\pi\cdot10^{-7}$	
Unit	Pa	T	kg/m^3	H/m	

As a general trend, fluid flows from right to left over one 40 ms cycle, but there are instants when a flow reversal is observed. On the other hand there is some amount of fluid that crosses the top boundary of domain. Also, a consistent vortex is noticeable at several moments over the cycle covering the central area swept by cilia. We conclude that, in the semi-infinite domain, an array of cilia can work both as a tool for fluid transportation along x-axis and as a tool for mixing. In order to distinguish which feature is

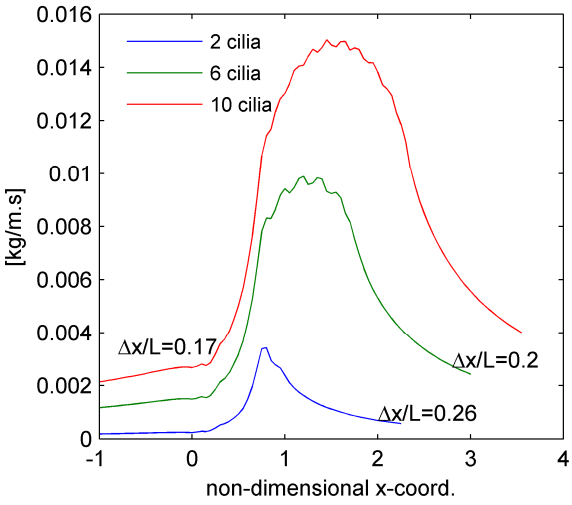

Figure 3. Averaged x-mass flow rate for different configurations.

prevailing on average and in what amount, we can define the transportation efficiency as

$$\varepsilon_T = \frac{\overline{\dot{m}}_x^L}{\overline{\dot{m}}_x^R} \qquad \overline{\dot{m}}_x = \frac{1}{t}\int_0^t \dot{m}_x(\tau)d\tau$$

where superscripts ^{L} and ^{R} stand for left and right boundaries of the computational domain. The time averaged x-mass flow rate versus x-coordinate for several configurations and minimum spacing is plotted in Figure 3. The minimum spacing is determined such that mechanical and geometrical equilibrium is ensured. The maximum mass boundary is attained for the minimum spacing corresponding to the configurations considered is illustrated in Figure 4. The efficiency ε_x depends on the

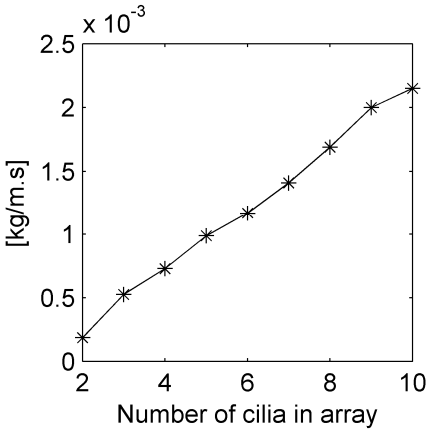

Figure 4. Maximum x-mass flow rate.

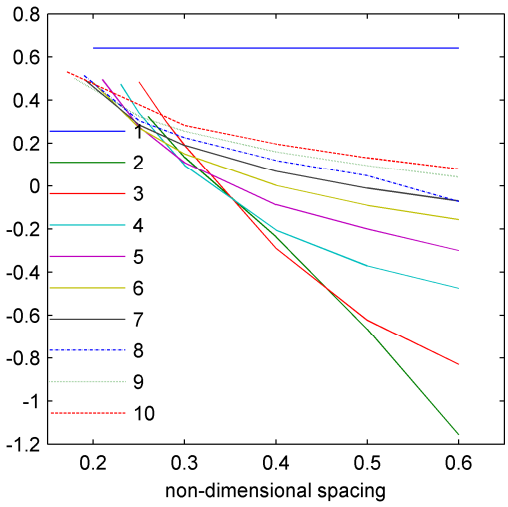

Figure 5. Transportation efficiency. Numbers in legend stand for number of cilia in array.

spacing among cilia $\Delta x / L$ and the number of cilia in array, as depicted in Figure 5. In the case of one-way mass flow rate the efficiency is positive. When fluid flows into the computational domain through both left and right boundaries the quantity is negative and is associated with the mixing process. The mass flow rate through the left boundary, $\overline{\dot{m}}_x^L$, increases with the number of cilia in array.

The behavior of transportation efficiency versus spacing is plotted in Figure 5. The most efficient configuration is that of a single cilium. In any other case, efficiency increases mainly with decreasing spacing. Increasing number of cilia in array induces only small rise in transportation efficiency.

Another interesting feature is the hydro-dynamical coupling (viscous coupling) among cilia which is the main responsible issue for metachronical coordination and wave-like pattern. In our case, meaning both asymmetric cilium geometry and driving engine, a metachronical coordination is less obvious. The frequency of the cilia array beats differs with less than 3% from the same quantity in the one cilium configuration. Also, wave-like pattern of the distal tips of the cilia, although present, is not so conspicuous as reported by Gueron and Levit-Gurevich, (1999).

What is really obvious is that the rightmost cilium in each array, no matter the number of constitutive entities, presents a different kinetic pattern. This pattern is influenced by the number of cilia in the array and the spacing. Figure 6 illustrates the orbits of the distal end of the rightmost cilium for different configurations and the same spacing. The same behavior but for identical configuration (6 cilia in array) and different spacing is shown in Figure 7. The inner cilia of the array (actually all other cilia except the last

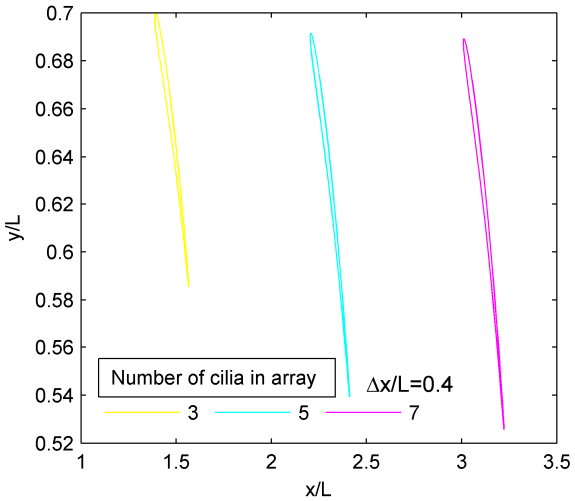

Figure 6. Orbits for rightmost cilium in 6 cilia array.

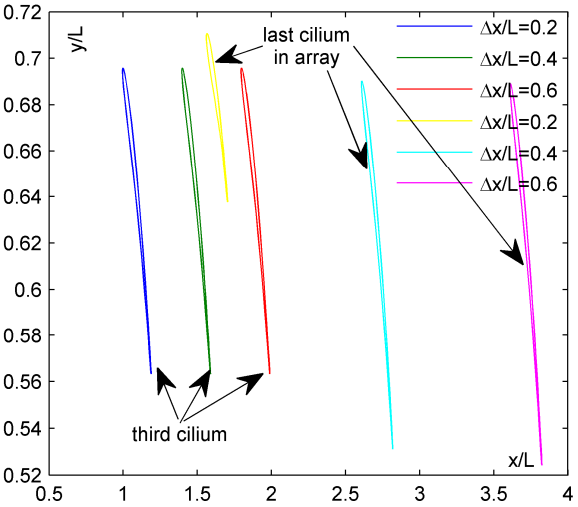

Figure 7. Comparison between orbits for inner and rightmost cilia in different configurations.

one) present the same kinematic behavior no matter the spacing.

These observations led us to associate this behavior with a system of rods and springs with a different spring constant for the last rod.

Further investigation needs to be performed.

5. Conclusions.

Rotating magnetic field is a viable possibility for actuating a battery of cilia in order to produce fluid transportation even in a semi-infinite domain. We expect better performance in a confined geometry. Beside number, cilia spacing is a crucial parameter that influences mass flow rate. Odd kinematic behavior is noticed for the first cilium in the array closest to the inlet boundary (on a time averaged basis).

Acknowledgements

This work has been supported through grant ARTIC FP6-2004-NMP-TI4.

References

Gueron, S., Liron, N., 1992. Ciliary motion modeling and dynamic multicilia interactions. Biophys. J., 63, 1045-1058.

Gueron, S., Levit-Gurevich, K., Liron, N., Blum, J.J., 1997. Cilia internal mechanism and metachronal coordination as the result of hydrodynamical coupling. Proc. Natl. Acad. Sci. USA, 94, pp 6001-6006, Applied Mathematics.

Gueron, S., Levit-Gurevich, K., 1998. Computation of the internal forces in cilia: Application to ciliary motion, the effects of viscosity and interactions. Biophys. J., 74, 1658-1676.

Gueron, S., Levit-Gurevich, 1999. Energetic considerations of ciliary beating and the advantage of metachronal coordination. Proc. Natl. Acad. Sci. USA, 96, no 2, pp 12240-12245, Applied Mathematics.

Isvoranu, D., Ioan, D., Parvu, P., 2008. Numerical simulation of single artificial cilium magnetic driven motion in a semi-infinite domain. Proceedings of the 1st European Conference on Microfluidics - Microfluidics 2008 - Bologna, paper 226.

Jackson, J.D., 1974. Classical Electrodynamics. John Wiley & Sons.